Applied Catalysis B: Environmental 147 (2014) 617–623

Contents lists available at ScienceDirect

Applied Catalysis B: Environmental

journal homepage: www.elsevier.com/locate/apcatb

Enhancing the photodegradation activity of n-type $WO_3 \cdot 0.33H_2O$ by proton-intercalation via negative potential biases

Yu-Cheng Hsiao [a], Yao-Hsuan Tseng [b], Chi-Chang Hu [a,*]

[a] Department of Chemical Engineering, National Tsing Hua University, 101, Section 2, Kuang-Fu Road, Hsin-Chu 30013, Taiwan
[b] Department of Chemical Engineering, National Taiwan University of Science and Technology, 43, Section 4, Keelung Road, Da'an District, Taipei City 106, Taiwan

ARTICLE INFO

Article history:
Received 9 July 2013
Received in revised form 3 September 2013
Accepted 22 September 2013
Available online 29 September 2013

Keywords:
Tungsten trioxide hydrate
Hydrothermal synthesis
Photocurrent density
Methylene blue de-colorization

ABSTRACT

It is here demonstrated that proton-intercalation via negative potential biases enhance the rate constant of methylene blue (MB) photo-electrocatalytic de-colorization on n-type tungsten trioxide hydrate ($WO_3 \cdot 0.33H_2O$ as prepared by hydrothermal synthesis), rather than the positive potential bias in promoting the charge separation of photo-generated electrons/holes. Due to the generation of W(V) and W(IV) hydroxyl species with smaller band gaps (in comparison with W(VI)) and the electrochemical activation of $WO_3 \cdot 0.33H_2O$, negatively biased proton intercalation into $WO_3 \cdot 0.33H_2O$ clearly enhances its photo-electrocatalytic activity for MB de-colorization, including its visible-light photo-electrocatalytic activity. A possible scheme for promoting the photocatalytic activity of $WO_3 \cdot 0.33H_2O$ through proton intercalation under constant potential biases is proposed and discussed. The photocatalytic de-colorization rate of MB on UV100-TiO_2 is significantly decreased under the same potential biases due to the difficulty in proton-intercalation

1. Introduction

Photocatalytic degradation of organic pollutants on semiconductors through solar energy is an important research field for environment protection and control. Extensive studies on the decomposition and mineralization of organic wastes or air pollutions such as dyes, bacteria, and NO_x, etc. have been conducted and several reviews have been published [1–5]. Among various materials, n-type semiconductors, such as TiO_2 [6], ZnO [7], and WO_3 [8], are widely employed to generate photo-excited electrons and holes for such applications. The underlying mechanisms of n-type semiconductor photocatalysis have been reviewed (see scheme SI in supplementary materials). The usage of suitable electron or hole scavengers, the presence of surface defect states, and the application of positively biased potentials are widely recommended for circumventing the problem of photo-generated electron/hole recombination.

Tungsten trioxide (WO_3) is an n-type, indirect band gap semiconductor with interesting photo-conducting behavior. This material also exhibits excellent electrochromic and photochromic properties, and has been extensively used in photocatalysis [8,9], electrochromic devices [10,11], supercapacitors [12], and gas sensors [13,14], etc. However, the potential of photo-generated electrons from WO_3 is too low to conduct hydrogen evolution [15]. Hence, combining n-type WO_3 and p-type Cu_2O has been employed for the solar water splitting application [16,17]. But due to its lower stability and activity compared with TiO_2, n-type WO_3 is rarely employed as a photocatalyst for organic degradation.

Among the various crystal structures of WO_3, hexagonal WO_3 leads to form large tunnels, which can be intercalated with cations to obtain hexagonal tungsten bronzes $M_\delta WO_3$ ($M = H^+, Li^+, Na^+$, etc.) with a blue color [18,19]. This phenomenon implies an enhanced solar efficiency for colored hexagonal tungsten bronzes in capturing visible light. This concept is supported by the recent finding that TiO_2 nanotubes show enhanced photocurrents by short-term-pulse Li^+ intercalation [20,21]. Since tungsten trioxide hydrate also exists in a hexagonal structure [22], proton intercalation into tungsten trioxide hydrate under negative biases rather than applying positive biases should enhance its solar efficiency in capturing visible-light photos and/or promote the electron/hole separation efficiency [23,24]. This idea was tested and the textural characteristics of $WO_3 \cdot 0.33H_2O$ prepared by the hydrothermal method are systematically investigated. The enhanced photo-electrocatalytic activity of $WO_3 \cdot 0.33H_2O$ by continuous proton intercalation through negative potential biases (rather than short-term electrochemical pulses) for dye de-colorization under both UV- and visible-light irradiation is clearly demonstrated in this work.

* Corresponding author. Tel.: +886 3 5736027; fax: +886 3 5736027.
E-mail address: cchu@che.nthu.edu.tw (C.-C. Hu).

0926-3373/$ – see front matter © 2013 Elsevier B.V. All rights reserved.
http://dx.doi.org/10.1016/j.apcatb.2013.09.041

2. Experimental details

2.1. $WO_3{\cdot}0.33H_2O$ preparation

$WO_3{\cdot}0.33H_2O$ powders were prepared by a mild hydrothermal synthesis process from a 30-mL aqueous solution containing 0.6 g $NaNO_3$ and 1.5 g $Na_2WO_4{\cdot}2H_2O$. The pH value of this solution was adjusted to 2.0 with 4 M H_2SO_4, which was transferred into a Teflon-lined autoclave with a stainless steel shell. This autoclave was heated to 180 °C at 10 °C min^{-1} in an oven. The autoclave was cooled to room temperature naturally after being maintained at 180 °C for 6 and 10 h. The products were obtained by centrifugation and washed with DI water several times to remove impurities. The obtained powders were then dried in an oven at 85 °C overnight (>8 h). Commercially available WO_3 (ACROS, monoclinic phase, PDF#71-214) and anatase TiO_2 (UV-100) are used as references.

2.2. Electrode preparation

For the electrode, 10 × 10 × 3 mm graphite (Nippon Carbon EG-NPL, N.C.K., Japan) was used as the substrate and its pre-treatment procedure completely followed our previous work [25]. First, 0.5 mg $WO_3{\cdot}0.33H_2O$ powders were well mixed with 5 wt% polyvinylidenefluoride (PVDF) and this mixture was supplemented with 40 μL C_5H_9NO under an ultrasonic bath. The suspension was dropped onto the substrate and dried at 85 °C. The exposed surface of the $WO_3{\cdot}0.33H_2O$-coated electrode is 1 cm^2 (insulated with polytetrafluoroethylene films) for the electrochemical-photocatalytic characterization.

2.3. Textural and photo-electrocatalytic characterization

X-ray diffraction (XRD) patterns were obtained from an X-ray diffractometer (Ultima IV, Rigaku) using a Cu target (Cu K_α = 1.5418 Å) at an angle speed of 1° (2θ) min^{-1} at 40 kV and 20 mA from 5° to 60°. The optic spectra were measured by a UV–Visible–NIR spectrophotometer (HITACHI, U-4100) from 200 to 2480 nm. The photocurrent densities against time under different potential biases and the photo-electrocatalytic de-colorization were conducted by an electrochemical analyser system CHI 1127A (CH Instruments, USA). An Ag/AgCl electrode (3 M KCl, Argenthal, 207 mV vs. SHE at 24 °C) was used as the reference and a platinum wire was employed as the counter electrode. A 150 W xenon lamp (Xe-150 specification, Labguide Co. Ltd) was used as the UV-light source. The visible light was generated from the same xenon light, filtered with a UV-cut off filter (Newport Resource Corporation FR-GG400), permeable wavelengths above 400 nm. The photocurrent density was measured in a three-electrode cell with a flat quartz window for light irradiation. The photocurrent density was measured in a 0.5 M Na_2SO_4 solution with pH = 2.0 at different negative potential biases from the open-circuit potential (E_{OCP}) to −0.4 V.

For the photo-electrocatalytic de-colorization of methylene blue (MB), the working electrode containing 0.5 mg cm^{-2} $WO_3{\cdot}0.33H_2O$ was submerged into a 20 mL 10 ppm MB solution with pH = 2.0 (adjusted with 4 M H_2SO_4) and set at the specified potential under stirring in darkness for 4 h to achieve the adsorption equilibrium. The counter electrode was a Pt sheet with an exposed surface area of 1 cm^2. Then, the photo-electrocatalytic de-colorization was conducted under UV- or visible-light irradiation. The MB concentration was determined from the absorbance at 664 nm by a UV–Vis spectrophotometer (SHIMADZU UV-2450) every 20 min.

2.4. Chemical oxygen demand analysis

Chemical oxygen demand (COD) was measured by the colorimetric method. A 2-mL testing solution was transferred into the potassium dichromate reagent (CHEMetrics K-7350S) as the oxidiser and digested at 150 °C for 2 h. The optical density for the colour of potassium dichromate was determined at 420 nm with an HACH spectrophotometer (HACH DR/4000U, Method 8000).

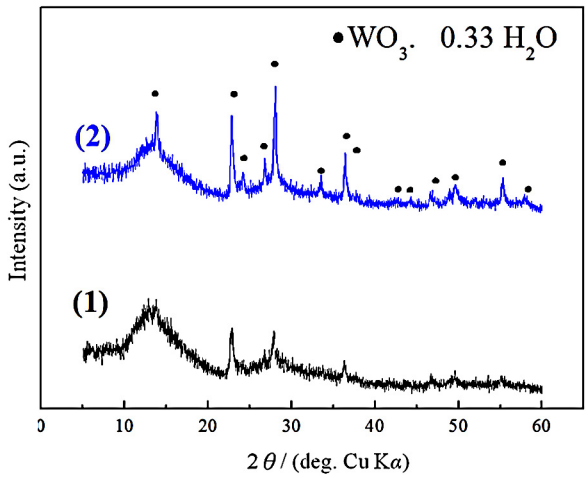

Fig. 1. X-ray diffraction patterns of $WO_3{\cdot}0.33H_2O$ with hydrothermal time = (1) 6 and (2) 10 h.

3. Results and discussion

3.1. Textural characteristics of $WO_3{\cdot}0.33H_2O$

Fig. 1 shows the XRD patterns of the as-prepared products. There are characteristic peaks centered at 14.1° (100), 22.9° (001), 24.4° (110), 27.0° (101), 28.3° (200), 33.7° (111), 36.6° (201), 43.3° (300), 44.6° (211), 46.8° (002), 49.2° (301), 50.1° (220), 55.6° (221), 57.6° (311) and 58.4° (400) on both patterns, and these reveal the presence of only one crystalline phase: $WO_3{\cdot}0.33H_2O$ (PDF#35-1001) in both samples. Therefore, 6-h hydrothermal time is long enough to obtain the crystalline phase of $WO_3{\cdot}0.33H_2O$. The Scherrer's equation is used to estimate the mean crystal size of $WO_3{\cdot}0.33H_2O$ from the full width at half maximum height of the main peak centered at 2θ = 28.3° and the results are shown in Table 1. Clearly, the mean crystal size of $WO_3{\cdot}0.33H_2O$ with the hydrothermal time equal to 6 h is smaller than that with 10 h. Furthermore, the BET data shown in Table 1 indicate that the $WO_3{\cdot}0.33H_2O$ powders with the hydrothermal time of 6 h exhibit a higher specific surface area. Due to the very similar standard XRD patterns of WO_3 (PDF#33-1387) and $WO_3{\cdot}0.33H_2O$ [26], the crystalline phase of tungsten oxide powders prepared in this work has been further confirmed by thermogravimetric and Raman analyses to be $WO_3{\cdot}0.33H_2O$ (see Fig. S1 in supplementary materials). Hereafter, $WO_3{\cdot}0.33H_2O$ powders with the hydrothermal times equal to 6 and 10 h are denoted as WO-6 and WO-10, respectively.

Fig. 2(a) shows the LSV curves of WO-6 and WO-10 measured at 2.5 mV s^{-1} in 0.5 M Na_2SO_4 with pH = 2.0 under darkness. In general, the LSV curves are similar in shape, while the current density of WO-6 is slightly larger than that of WO-10, especially for the peak at ca. −0.2 V. The former result is probably due to that WO-6 and WO-10 consist of the same compound: $WO_3{\cdot}0.33H_2O$. The latter result

Table 1
Grain size and specific surface area of $WO_3{\cdot}0.33H_2O$ prepared by hydrothermal synthesis.

Hydrothermal time (h)	Grain size (nm)	Surface area (m^2 g^{-1})
6	16.20	54.9
10	32.00	48.6

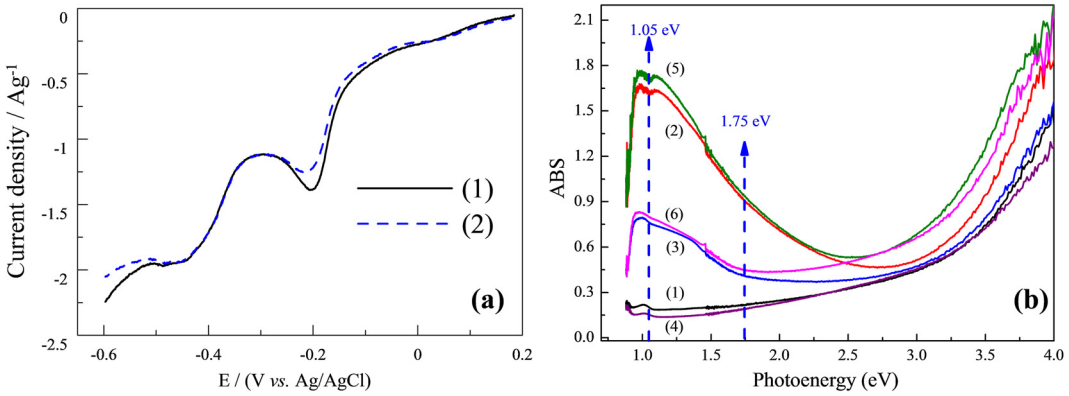

Fig. 2. (a) LSV curves of (1) WO-6 and (2) WO-10 measured at 2.5 mV s^{-1} in 0.5 M Na_2SO_4 with pH = 2.0 under darkness. (b) The *ex-situ* UV–VIS–NIR absorption spectra of (1–3) WO-6 and (4–6) WO-10 biased at (1,4) open-circuit potential, (2,5) −0.4 V, and (3,6) −0.1 V.

suggests that WO-6 is more electroactive than WO-10, attributable to a higher specific surface area and/or smaller crystal size. Note that both curves show an unclear wave at 0 V, a sharp reduction peak centered at −0.2 V, and a broad shoulder from −0.32 to −0.5 V, corresponding to the reduction of $WO_3{\cdot}0.33H_2O$ involving proton intercalation since no visible hydrogen bubbles found as potentials are swept to −0.6 V. The proton intercalation into tungsten trioxide hydrate can be simply expressed as Eq. (1) [27]:

$$WO_3 \cdot 0.33H_2O + \delta e^- + \delta H^+ \leftrightarrow H_\delta WO_3 \cdot 0.33H_2O \quad (1)$$

where the degree of proton intercalation depends on the negatively biased potential. Based on Eq. (1), WO-6 and WO-10 polarized at −0.1 and −0.4 V will reduce certain W(VI) species to generate the W(V) and/or W(IV) hydroxyl species within $WO_3{\cdot}0.33H_2O$, which are visible-light and near-IR sensitive.

Fig. 2(b) shows the *ex-situ* UV–Vis–NIR spectra of WO-6 and WO-10 polarized at −0.1 or −0.4 V for 10 min in 0.5 M Na_2SO_4 with pH = 2. After polarization, the electrode was moved to the UV–Vis–NIR spectrophotometer within 5 min to obtain its spectrum. In general, the UV–Vis–NIR spectra of WO-6 and WO-10 under the same biased state are very similar in shape, probably due to that WO-6 and WO-10 consist of the same compound. For WO-6 and WO-10 under the open-circuit potential state (*i.e.*, without potential bias), the two UV–Vis–NIR spectra almost overlap in the whole wavelength region. Since the difference between WO-6 and WO-10 is the crystal size and the specific surface area, the above result suggests that both factors show only minor effects on the light-absorption ability of $WO_3{\cdot}0.33H_2O$. Moreover, the absorbance in the near-IR region is minor while the absorption becomes stronger with the shift to shorter wavelengths (*i.e.*, increasing the photo-energy). These results indicate that the visible light-absorption ability of as-prepared $WO_3{\cdot}0.33H_2O$ is not strong, probably resulting in its negligible visible-light photocatalytic activity to the MB degradation (see below). When the electrode potential is negatively shifted to −0.1 V, an obvious absorption band can be found between 0.95 and 2.5 eV on both samples. In addition, the intensity of this band increases with the more negative bias (−0.4 V) of $WO_3{\cdot}0.33H_2O$. The above phenomena reveal that proton intercalation into $WO_3{\cdot}0.33H_2O$ enhances the near-IR and visible-light absorption of $WO_3{\cdot}0.33H_2O$. On the other hand, under the same polarization state (*e.g.*, at −0.1 V), the absorbance from 1.75 to 4.0 eV for WO-10 is stronger than that for WO-6, suggesting that the memory effect of $WO_3{\cdot}0.33H_2O$ with a larger crystal size (*i.e.*, WO-10) is more obvious than that with a smaller crystal size. This statement is supported from a comparison of the UV–Vis–NIR spectra of WO-6 biased at −0.1 and −0.4 V; where enhanced absorbance from 2.75 to 4.0 eV is clearly visible for the sample polarized at −0.4 V. Note that the color of $WO_3{\cdot}0.33H_2O$ coatings was clearly changed from gray to blue when WO-6 and WO-10 were biased at −0.4 V, even when the polarization had been interrupted (*i.e.*, a memory effect). According to the report by Ozkan et al. [28], the blue-colored WO_3 contains W(IV), W(V), and W(VI) states and the optical absorption was influenced by the small polaron transition among these three valence states of tungsten oxide. In addition, the band centered around 1.05 eV might be attributed to the small polaron transition between W(VI) and W(V) states meanwhile the band centered around 1.75 eV should result from the polaron transition between W(V) and W(IV) states. Also note that from a comparison among curves 1–3 (or curves 4–6), proton intercalation into $WO_3{\cdot}0.33H_2O$ significantly promotes the optical absorption not only in the near-IR region but also in the visible- and UV-light regions. Accordingly, the cathodic proton intercalation at negatively biased potentials can be considered an electrochemical activation step to generate photoactive W hydroxyl species and more oxygen-deficiency sites within $WO_3{\cdot}0.33H_2O$, which work as electron donors [23,24].

3.2. Photo-electrocatalytic de-colorization of MB

The current density against time at a biased potential of −0.4 V under the repeated light-on/-off test for WO-6 and WO-10 are shown in the Supplementary materials (see Fig. S2 and corresponding descriptions). In order to gain a more detailed understanding on the photo-electrochemical responses of $WO_3{\cdot}0.33H_2O$, the typical photo-electrochemical responses of WO-6 are shown in Fig. 3(a). Note that a pseudo-steady-state current density of ca. −373 μA cm^{-2} before the repeated light-on/-off test is obtained. When the light source is applied, the resultant current density decreases to a minimum of −345 μA cm^{-2} (in magnitude), and then an obvious increase in the cathodic current density is clearly found. The above decrease in the cathodic current density as light is applied indicates the presence of anodic photocurrents under the UV-light irradiation. This result reveals the n-type semiconductor characteristics of $WO_3{\cdot}0.33H_2O$. The further increase in the cathodic current density is due to a combined photo-electrochemical process on $WO_3{\cdot}0.33H_2O$ (see below). In general, the photocurrent density of an n-type semiconductor (*e.g.*, TiO_2) will be increased by the positive shift in the photo-anode potential because of the significant reduction in the electron/hole recombination rate, meanwhile a steady-state anodic photocurrent appeared immediately when the light source was turned on [29,30]. It is noteworthy that the average photocurrent density of WO-6 was steadily increased from 4.135 to 33.415 μA cm^{-2} when the potential bias was negatively shifted from −0.1 to −0.4 V (see Table 2). This phenomenon could be attributed to the fact that under a more negative potential bias, $WO_3{\cdot}0.33H_2O$ is electrochemically reduced

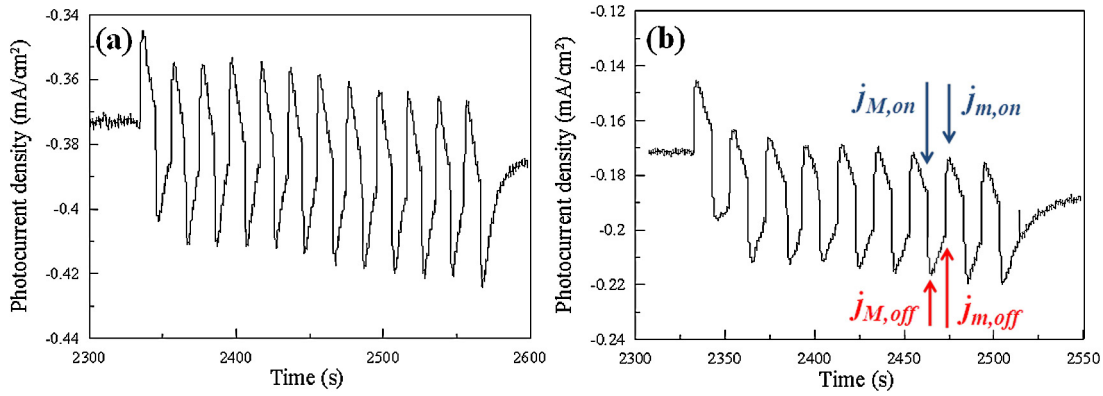

Fig. 3. Current responses of (a) WO-6 and (b) WO-10 biased at −0.4 V. The current fluctuation is due to the repeated 10-s light-on/-off photo-electrochemical test.

to form more W(IV) and W(V) species to increase the photosensitive species. Hence, the more negative potential bias is applied, the higher photocurrent density of $WO_3{\cdot}0.33H_2O$ is obtained. Accordingly, the mechanism of enhancing the photocurrent density of this n-type $WO_3{\cdot}0.33H_2O$ via the negative potential bias is different from that of common n-type semiconductors which generally show a higher photocurrent density under positive potential biases. Also note that to avoid any hydrogen evolution on $WO_3{\cdot}0.33H_2O$, the most negative potential acceptable to $WO_3{\cdot}0.33H_2O$ is set at −0.4 V.

The average photocurrent density of $WO_3{\cdot}0.33H_2O$ shown in Table 2 is defined as Eq. (2):

$$j = \frac{\sum_{i=1}^{n}[(j_{m,off} - j_{m,on}) + (j_{M,off} - j_{M,on})]_i}{2n} \quad (2)$$

where $j_{m,off}$, $j_{m,on}$, $j_{M,off}$, and $j_{M,on}$ are indicative of the current density of the minimum under light-off, the current density of the minimum under light-on, the current density of the maximum under light-off, and the current density of the maximum under light-on, respectively (in magnitude, see Fig. 3(b)). The average photocurrent density was repeatedly measured 4 times while the photocurrent density was stable in the 1-h (or longer) test.

As described previously, when the current density reaches the minimum under light irradiation, an obvious increase in the cathodic current density is clearly found (*i.e.*, from $j_{m,on}$ to $j_{M,on}$ in every light-on period). This unusual phenomenon is attributable to a combination of two processes. First, $WO_3{\cdot}0.33H_2O$ was reduced electrochemically to form $H_\delta WO_3{\cdot}0.33H_2O$ under a negative potential bias and the rate of proton intercalation into $WO_3{\cdot}0.33H_2O$ should depend on the applied potential. Second, under UV-light irradiation, the excited photoelectrons were transferred to the circuit to oppose the reduction current applied to $WO_3{\cdot}0.33H_2O$. The obvious increase in the cathodic current density after the current density reaches the minimum under the UV-light irradiation probably indicates that the driving force of electrochemical reduction is stronger than that of photo-excitation on $WO_3{\cdot}0.33H_2O$.

To demonstrate the variation in the photo-electrocatalytic degradation activity of $WO_3{\cdot}0.33H_2O$ under cathodic polarization, WO-6 and WO-10 biased at various potentials were employed to decolorize MB (10 mg L^{-1} MB). Fig. 4 shows the comparison of photo-electrocatalytic de-colorization rate of MB on WO-6 and WO-10 biased at different potentials under UV-light irradiation. From an examination of these six curves, several features should be emphasized. First, the photo-electrocatalytic de-colorization of MB follows the pseudo-first order rate law. This phenomenon suggests a similar de-colorization mechanism on $WO_3{\cdot}0.33H_2O$ with different potential biases. Second, the rate of MB de-colorization on WO-6 is faster than that on WO-10 when the applied potential is the same. This trend is consistent with the results of average photocurrent density shown in Table 2. Hence, WO-6 biased at −0.4 V shows the highest photo-electrocatalytic activity for MB de-colorization among the above six tests. The higher photo-electroocatalytic activity of WO-6 is reasonably attributed to its higher specific surface area in comparison with WO-10, which contains more active sites to de-colorize MB. Third, the order of potential bias with respect to decreasing the de-colorization rate for WO-6 and WO-10 is: −0.4 V > open-circuit potential > −0.1 V. This order, however, is different from that of the average photocurrent density obtained at different potential biases. This conflict probably results from the combination of two effects. (i) The proton-intercalation enhancement in the photosensitivity of $WO_3{\cdot}0.33H_2O$ is relatively minor when the potential bias is set at −0.1 V. This statement is supported by the average photocurrent density is smaller than 5 μA cm^{-2} when WO-6 and WO-10 were set at the open-circuit potential and −0.1 V (see Table 2). Hence, the number of photo-excited electrons and holes was not significantly increased and might be easily recombined within $WO_3{\cdot}0.33H_2O$

Table 2
Average photocurrent density of $WO_3{\cdot}0.33H_2O$ measured at various potential biases.

Semiconductor	Average photocurrent density (μA cm^{-2})				
	−0.4 (V)	−0.3 (V)	−0.2 (V)	−0.1 (V)	OCP
WO-6	33.415	18.083	14.565	4.135	0.328
WO-10	30.828	16.025	7.898	2.520	0.249

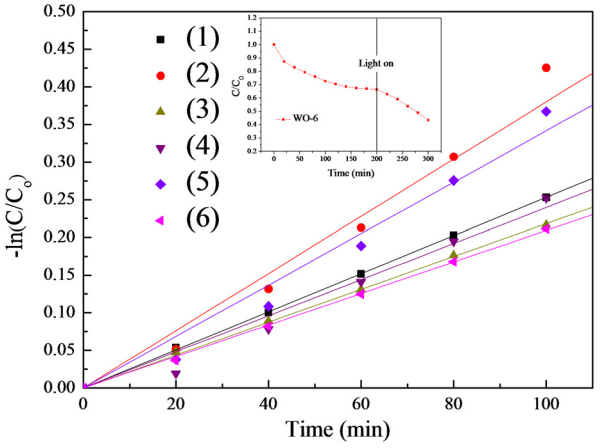

Fig. 4. MB de-colorization curves under the UV-light irradiation for (1–3) WO-6 and (4–6) WO-10 at a potential bias of (1,4) open-circuit potential, (2,5) −0.4 and (3,6) −0.1 V. (Inset: time-course of the changes in concentration of MB in the presence of WO-6 at a potential bias of −0.4 V).

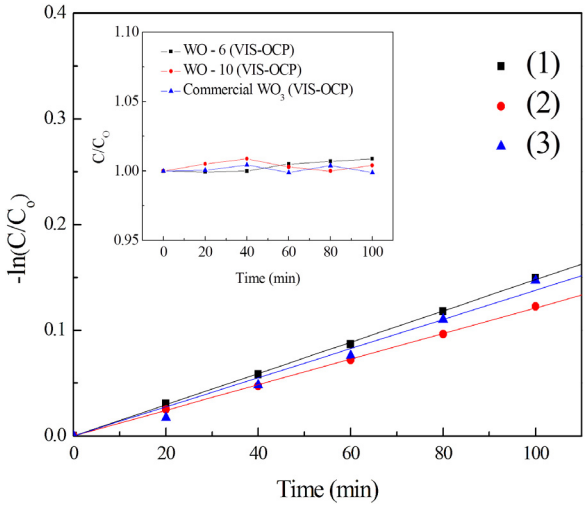

Fig. 5. MB de-colorization curves under visible-light illumination for (1) WO-6, (2) WO-10, and (3) commercial WO_3 at a potential bias of −0.4 V.

[31]. (ii) $WO_3{\cdot}0.33H_2O$ is an n-type semiconductor and its photo-electrocatalytic activity should be enhanced by a positive potential bias because of more efficient electron/hole separation at a more positive potential bias. On the other hand, the much higher de-colorization rate of $WO_3{\cdot}0.33H_2O$ (both WO-6 and WO-10) biased at −0.4 V supports the proton-intercalation enhancement in the photo-electrocatalytic de-colorization activity of $WO_3{\cdot}0.33H_2O$. This phenomenon indicates that the effect of the electrochemical generation of photoactive species (*i.e.*, the W hydroxyl species with absorption around 1.05 and 1.75 eV and the enhanced absorbance at the photo-energy above 2.5 eV from Fig. 2) on promoting the MB decomposition rate is stronger than that of a more negative potential on the electron/hole recombination.

Fig. 5 shows the typical MB de-colorization curves under the visible-light irradiation on WO-6 and WO-10 with a negative potential bias at −0.4 V. Clearly, WO-6 and WO-10 biased at −0.4 V exhibit obvious photo-electrocatalytic activities to MB de-colorization under the visible-light irradiation. Moreover, the de-colorization activity of WO-6 is higher than that of WO-10. This phenomenon is consistent with the results of photocurrent density and UV–Vis–NIR spectra shown in Table 2 and Fig. 2(b). On the other hand, both WO-6 and WO-10 do not show visible-light-driven photocatalytic ability to MB de-colorization when both oxides are under the open-circuit state (see inset in Fig. 5). This result clearly demonstrates that proton intercalation into $WO_3{\cdot}0.33H_2O$ enhances its near-IR and visible-light absorption, activating the visible-light-driven photocatalytic activity of $WO_3{\cdot}0.33H_2O$ for MB de-colorization. For the reference sample, the photo-electrocatalytic activity of commercial WO_3 under UV-light irradiation is similar to that of $WO_3{\cdot}0.33H_2O$ prepared in this work (see Table 3). In addition, commercial WO_3 also shows similar proton-intercalation enhancement in the visible-light-driven photocatalytic activity for MB de-colorization.

Table 3
Rate constant for the pseudo-first order rate law of MB photo-electrocatalytic de-colorization on $WO_3{\cdot}0.33H_2O$-, commercial WO_3- and UV100-coated electrodes under the UV-light irradiation at various potential biases.

Semiconductor	Rate constant ($1\ min^{-1}$)		
	E_{ocp}	−0.4 (V)	−0.1 (V)
WO-6	0.00253	0.00380	0.00218
WO-10	0.00240	0.00342	0.00209
Commercial WO_3	0.00210	0.00318	0.00223
UV100	0.0308	0.00215	0.00229

In general, the photocatalytic de-colorization activity of an n-type semiconductor, such as UV100-TiO_2 should increase with a positive potential bias because the recombination of photo-generated electrons and holes could effectively be hindered by the positive potential bias. Therefore, the photocatalytic de-colorization rate of MB on a UV100-coated electrode is significantly decreased under the negative potential bias. Such a phenomenon is clearly demonstrated in Table 3, where the photo-electrocatalytic de-colorization of MB has been performed on a UV100-coated electrode with negative potential biases of −0.1 and −0.4 V. Accordingly, it is reasonable that the rate constant of MB de-colorization is smaller with a more negatively biased potential. This decrease in the photocatalytic de-colorization activity of UV100–TiO_2 under the same potential biases is attributed to its difficulty in proton-intercalation at potentials less negative than −1.0 V.

Based on the above comparison, a schematic pathway for promoting the photo-electrocatalytic activity of $WO_3{\cdot}0.33H_2O$ by proton intercalation is expressed as Scheme 1. Here, the as-prepared $WO_3{\cdot}0.33H_2O$ is not significantly sensitive to the visible light (from Fig. 2(b), state 1). Through the proton intercalation, this compound became a visible-light-driven photocatalyst (state 2). Moreover, the above electrochemical activation produced more photo-sensitive W(IV), W(V), and W(VI) species in $WO_3{\cdot}0.33H_2O$. Hence, with a more negative potential bias, a higher photocurrent density of $WO_3{\cdot}0.33H_2O$ was obtained. Since reduction currents were applied to the $WO_3{\cdot}0.33H_2O$ photo-electrode, oxidation reaction(s) should occur on the Pt electrode. Because the UV–Vis spectra of the MB solution approximately overlapped in the overall wavelength region when the adsorption time was longer than 3 h, the small anodic current density on the Pt counter electrode could not effectively decompose MB. On the other hand, when the photo-electrode was irradiated with UV- or visible-light (state 3), the photo-excited electrons would be pushed back to $WO_3{\cdot}0.33H_2O$ and further activated $WO_3{\cdot}0.33H_2O$. Meanwhile, a portion of the electrons and holes may react with O_2 and water/OH^- to generate highly active species (*e.g.*, $O_2^{-}\cdot$ or $OH\cdot$) to de-colorize the MB solution although the negatively biased potentials would favor the recombination of photo-excited electron/hole pairs. In summary, proton intercalation into $WO_3{\cdot}0.33H_2O$ enhances its near-IR, visible-light, and UV-light absorption and also activates its UV- and visible-light-driven photocatalytic activities for MB de-colorization. This is more effective than applying positively biased potentials to reduce the recombination of photo-excited electrons/holes.

Fig. 6 shows the results of COD retention and MB concentration retention in a standard MB testing solution that was subjected to the photo-electrocatalytic de-colorization on a WO-6-coated electrode biased at −0.4 V for 4 h in darkness and then under the UV-light irradiation for 100 min. A comparison of the COD and MB concentration retention is useful to gain the oxidation ability of the photo-electrocatalytic de-colorization in this work since COD is an index evaluating the average oxidation state of pollutants [32]. The reductions in the MB concentration and COD are, respectively, equal to 33.90% and 19.79% in the 4-h adsorption process (under darkness) with the potential biased at −0.4 V. Since the 4-h adsorption of MB consumed about 12.72% of the MB when the adsorption was performed without potential biases, 21.18% MB should be consumed by the electrochemical oxidation for 4 h. Moreover, the COD removal efficiency, defined as the ratio between the COD removal and the decrease in the MB concentration, for this pure adsorption process should be 100%. Accordingly, the COD removal efficiency purely due to the electrochemical oxidation was about 33.38% in the 4-h adsorption process with the potential biased at −0.4 V. In the photo-electrocatalytic process for 100 min, on the other hand,

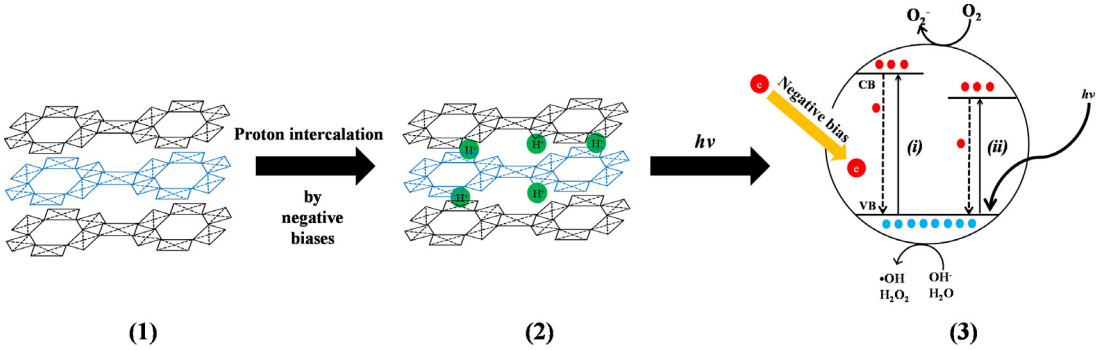

Scheme 1. Schematic route for promoting the photo-electrocatalytic activity of $WO_3{\cdot}0.33H_2O$: (1) under the open-circuit state, (2) proton intercalation and electrochemical activation by negative potential biases, and (3) photo-electrocatalytic de-colorization of MB on $WO_3{\cdot}0.33H_2O$ with proton intercalation: (*i*) enhancement in the UV-light absorption region and (*ii*) creation of new bands with band gap from ca. 2 5 to 0.95 eV in the visible-light absorption region.

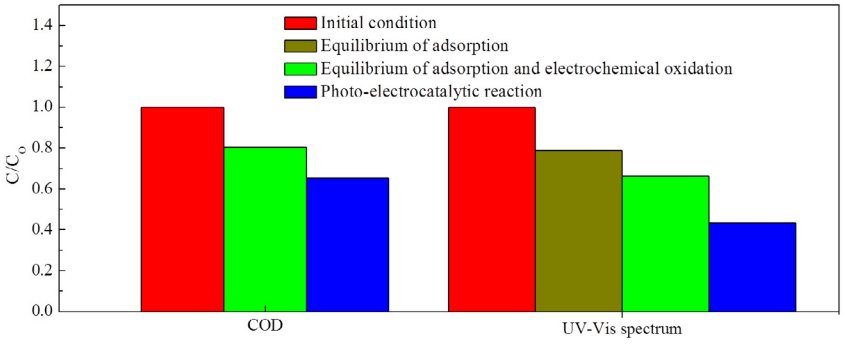

Fig. 6. COD retention (left) and MB concentration retention (right) of the standard testing solution with the photo-electrocatalytic de-colorization on WO-6 biased at −0.4 V for 4 h in darkness and then under the UV-light irradiation for 100 min.

the decreases in MB concentration and COD were about 22.93% and 15.0%, respectively. Accordingly, the COD removal efficiency in the photo-electrocatalytic de-colorization process was equal to 65.42%. The above results clearly demonstrate the high COD removal efficiency of the photo-electrocatalytic process. Based on the ratio of COD and MB removal, both the auxo-chromic group and main chain of MB are decomposed to form certain oxidized intermediates during the photo-electrocatalytic process. This evidence supports the proposal that highly active species such as $O_2^{-\bullet}$ or $OH^\bullet$ radicals are formed to decompose the MB molecules during the process of photo-electrocatalytic de-colorization.

3.3. *Influences of methylene blue*

There is a doubt that organic dyes may act as photo-sensitizers to change the photo-electrocatalytic activity of MB de-colorization in this combined electro-chemical and photocatalytic system [33]. To clarify the possible influences of methylene blue on the photo-electrocatalytic de-colorization process, the photo-electrochemical responses of $WO_3{\cdot}0.33H_2O$ was further evaluated by the photo-electrochemical tests in the 0.5 M Na_2SO_4 solution (pH = 2) with and without 10 ppm MB under visible-light irradiation. Fig. 7 shows the typical chronoamperometric curves measured in the above two solutions. From a comparison of these two curves, although the responses are similar in shape, several features should be mentioned. First, the pseudo-steady-state current density before light irradiation is decreased by adding MB into the Na_2SO_4 solution. Clearly, the background current due to proton intercalation into WO-6 is significantly depressed by the MB adsorption. This phenomenon is visible over the whole test period, *i.e.*, the approximately constant difference in the response current density between two curves under light-off. Second, under the visible-light irradiation, a decrease in the cathodic current density is found on both curves, revealing the n-type semiconductor characteristics of WO-6. Third, if the adsorbed MB could act as a photo-sensitizer, a larger photo-excited current density generated from WO-6 and adsorbed MB should be found and a larger difference in the current density between light-on and light-off should be observed in the solution containing MB. However, the photocurrent density is slightly depressed by the MB adsorption, revealing that no photo-excited electrons on the adsorbed MB can be injected into WO-6. Moreover, the adsorbed MB should shield the visible light, causing the slight decrease in the photocurrent density. Based on the above results and discussion, it is clear that MB does not act as a photo-sensitizer to promote the photo-electrocatalytic de-colorization efficiency of $WO_3{\cdot}0.33H_2O$.

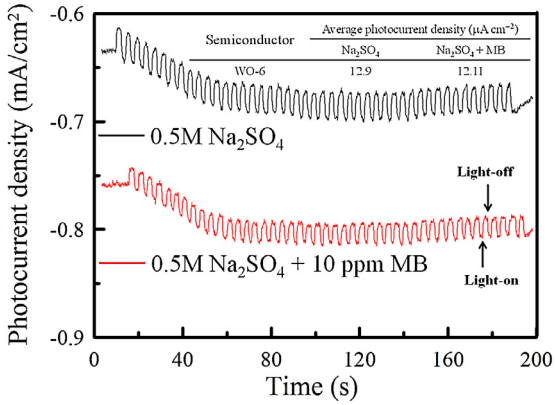

Fig. 7. Photocurrent density responses measured at −0.4 V in 0.5 M Na_2SO_4 (pH = 2) without and with 10 ppm MB under the visible-light irradiation.

4. Conclusions

Continuous proton-intercalation via negative potential biases enhances the photo-electrocatalytic activity of n-type $WO_3{\cdot}0.33H_2O$ on MB de-colorization. The crystal size and specific surface area of $WO_3{\cdot}0.33H_2O$ are changed by varying the hydrothermal time. The $WO_3{\cdot}0.33H_2O$ with smaller crystal size and larger specific surface area exhibits a larger average photocurrent density. Such $WO_3{\cdot}0.33H_2O$ nanocrystals negatively biased at −0.4 V shows the highest photocurrent density and largest rate constant of MB de-colorization. The proton intercalation into $WO_3{\cdot}0.33H_2O$ significantly promotes the optical absorption not only in the near-IR region but also in the visible- and UV-light regions, which is an electrochemical activation step to generate more photoactive W hydroxyl species to degrade organics. At potentials positive to −0.4 V, with more negatively biased potential, there is higher photo-electrocatalytic activity of $WO_3{\cdot}0.33H_2O$. In comparison with the case measured in 0.5 M Na_2SO_4 (pH = 2), the slightly smaller photocurrent density of $WO_3{\cdot}0.33H_2O$ obtained in the same solution containing MB reveals that MB cannot act as a photo-sensitizer to promote the photo-electrocatalytic de-colorization activity of $WO_3{\cdot}0.33H_2O$. From the COD removal efficiency, both the auxo-chromic group and main chain of MB were degraded to form certain oxidised intermediates during the photo-electrocatalytic de-colorization process.

Acknowledgements

The financial supports of this work, the National Science Council of ROC-Taiwan (NSC 100-2628-E-007-028-MY2), the Ministry of Economic Affairs of ROC-Taiwan (MEA 101-EC-17-A-08-S1-208), and the boost program from the LCERC of NTHU, are gratefully acknowledged.

Appendix A. Supplementary data

Supplementary data associated with this article can be found, in the online version, at http://dx.doi.org/10.1016/j.apcatb.2013.09.041.

References

[1] J. Luo, M. Hepel, Electrochim. Acta 46 (2001) 2913–2922.
[2] W. Zhou, G. Du, P. Hu, Y. Yin, J. Li, J. Yu, G. Wang, J. Wang, H. Liu, J. Wang, H. Zhang, J. Hazard. Mater. 197 (2011) 19–25.
[3] Y.C. Hsiao, Y.H. Tseng, Micro Nano Lett. 5 (2010) 317–320.
[4] Y. Hou, J. Qu, X. Zhao, P. Lei, D. Wan, C.P. Huang, Sci. Total Environ. 407 (2009) 2431–2439.
[5] C. Huang, W.P. Hsieh, J.R. Pan, S.M. Chang, Sep. Purif. Technol. 58 (2007) 152–158.
[6] A.L. Linsebigler, G. Lu, J.T. Yates Jr., Chem. Rev. 95 (1995) 735–758.
[7] L. Wan, X. Li, Z. Qu, Y. Shi, H. Li, Q. Zhao, G. Chen, J. Hazard. Mater. 184 (2010) 864–868.
[8] J. Yu, L. Qi, J. Hazard. Mater. 169 (2009) 221–227.
[9] K. Sayama, H. Hayashi, T. Arai, M. Yanagida, T. Gunji, H. Sugihara, Appl. Catal., B 94 (2010) 150–157.
[10] J. Livage, D. Ganguli, Sol. Energy Mater. Sol. Cells 68 (2001) 365–381.
[11] C.C. Liao, F.R. Chen, J.J. Kai, Sol. Energy Mater. Sol. Cells 90 (2006) 1147–1155.
[12] K.H. Chang, C.C. Hu, C.M. Huang, Y.L. Liu, C.-I. Chang, J. Power Sources 196 (2011) 2387–2392.
[13] I. Jiménez, J. Arbiol, G. Dezanneau, A. Cornet, J.R. Morante, Sens. Actuators, B 93 (2003) 475–485.
[14] J. Tamaki, Z. Zhang, K. Fujimori, M. Akiyama, T. Harada, N. Miura, N. Yamazoe, J. Electrochem. Soc. 141 (1994) 2207–2210.
[15] Y.P. Xie, G. Liu, L. Yin, H.M. Cheng, J. Mater. Chem. 22 (2012) 6746–6751.
[16] C.C. Hu, J.N. Nian, H. Teng, Sol. Energy Mater. Sol. Cells 92 (2008) 1071–1076.
[17] J.N. Nian, C.C. Hu, H. Teng, Int. J. Hydrogen Energy 33 (2008) 2897–2903.
[18] J.D. Guo, K.P. Reis, M.S. Whittingham, Solid State Ionics 53–56 (1992) 305–314.
[19] K. Huang, Q. Pan, F. Yang, S. Ni, X. Wei, D. He, J. Phys. D: Appl. Phys. 41 (2008) 155417 (6pp).
[20] B.H. Meekins, P.V. Kamat, ACS Nano 3 (2009) 3437–3446.
[21] U. Kang, H. Park, Appl. Catal., B 140–141 (2013) 233–240.
[22] L. Seguin, M. Figlarz, Solid State Ionics 63–65 (1993) 437–441.
[23] H. Zheng, J.Z. Ou, M.S. Strano, R.B. Kaner, A. Mitchell, K. Kalantar-zadeh, Adv. Funct. Mater. 21 (2011) 2175–2196.
[24] E. Wahlström, E.K. Vestergaard, R. Schaub, A. Rønnau, M. Vestergaard, E. Lægsgaard, I. Stensgaard, F. Besenbacher, Science 303 (2004) 511–513.
[25] C.C. Hu, W.Y. Li, J.Y. Lin, J. Power Sources 137 (2004) 152–157.
[26] J.H. Ha, P. Muralidharan, D.K. Kim, J. Alloys Compd. 475 (2009) 446–451.
[27] Z. Xie, L. Gao, B. Liang, X. Wang, G. Chen, Z. Liu, J. Chao, D. Chen, G. Shen, J. Mater. Chem. 22 (2012) 19904–19910.
[28] E. Ozkan, S.H. Lee, C.E. Tracy, J.R. Pitts, S.K. Deb, Sol. Energy Mater. Sol. Cells 79 (2003) 439–448.
[29] W. Li, J. Li, X. Wang, J. Ma, Q. Chen, Int. J. Hydrogen Energy 35 (2010) 13137–13145.
[30] M. Hepel, J. Luo, Electrochim. Acta 47 (2001) 729–740.
[31] J. Guo, Y. Li, S. Zhu, Z. Chen, Q. Liu, D. Zhang, W.J. Moon, D. Song, RSC Adv. 2 (2012) 1356–1363.
[32] R.A. Torres, F. Abdelmalek, E. Combet, C. Pétrier, C. Pulgarin, J. Hazard. Mater. 146 (2007) 546–551.
[33] J.M. Herrmann, Appl. Catal., B 99 (2010) 461–468.